Journal of
Applied Crystallography
ISSN 0021-8898

Received 16 August 2006
Accepted 30 October 2006

A new experimental station for simultaneous X-ray microbeam scanning for small- and wide-angle scattering and fluorescence at BESSY II

Oskar Paris,[a]* Chenghao Li,[a] Stefan Siegel,[a] Gundolf Weseloh,[a,b] Franziska Emmerling,[c] Heinrich Riesemeier,[c] Alexei Erko[d] and Peter Fratzl[a]

[a]Department of Biomaterials, Max Planck Institute of Colloids and Interfaces, D-14424 Potsdam, Germany, [b]Institute of Applied Physical Chemistry, University of Heidelberg, D-69120 Heidelberg, Germany, [c]Federal Institute for Materials Research and Testing, D-12205 Berlin, Germany, and [d]BESSY GmbH, D-12489, Germany. Correspondence e-mail: oskar.paris@mpikg.mpg.de

A new instrument for simultaneous microbeam small- and wide-angle X-ray scattering and X-ray fluorescence (SAXS/WAXS/XRF) is presented. The instrument is installed at the microfocus beamline at BESSY II and provides a beam of 10 μm size with a flux of about 10^9 photons s^{-1}. A SAXS resolution up to 500 Å *d*-spacing and a range of scattering vectors of almost three orders of magnitude are reached by using a large-area high-resolution CCD-based detector for simultaneous SAXS/WAXS. The instrument is particularly suited for scanning SAXS/WAXS/XRF experiments on hierarchically structured biological tissues. The necessary infrastructure, such as a cryo-stream facility and an on-site preparation laboratory for biological specimens, are available.

1. Introduction

Hard X-ray microbeams from third-generation synchrotron radiation sources have become routinely feasible in recent years due to the high source brilliance and many outstanding developments in X-ray optics. Among other techniques, such microbeams are important tools in position-resolved small- and wide-angle X-ray scattering (SAXS and WAXS) on condensed matter (Riekel, 2000). In particular, the two-dimensional mapping of nanostructural parameters derived from two-dimensional SAXS/WAXS patterns has become a key technique to investigate hierarchically structured nanocomposites such as, for instance, polymer fibres (Riekel & Davies, 2005), carbon fibres (Loidl *et al.*, 2005) and biological tissues (Paris *et al.*, 2000; Fratzl, 2003). For hierarchically structured biological tissues, detailed knowledge of the structure at all hierarchical levels is of outstanding importance for the understanding of structure–property relationships (Weiner & Wagner, 1998; Currey, 1999; Kamat *et al.*, 2000; Fratzl *et al.*, 2004; Aizenberg *et al.*, 2005). Thus, scanning SAXS/WAXS experiments on hierarchical tissues such as bone or wood require a beam size adapted to the hierarchical level of interest. Several studies have been performed so far with laboratory equipment with beam sizes of ≈ 200 μm (Fratzl *et al.*, 1997; Jaschouz *et al.*, 2003), and with synchrotron radiation with beam sizes from ≈ 20 μm (Žižak *et al.*, 2000; Žižak *et al.*, 2003) down to about 1 μm (Lichtenegger *et al.*, 1999; Wagermaier *et al.*, 2007) in recent years. The principle of the technique having been well demonstrated and elaborated, one of the needs is now to install dedicated synchrotron instruments for routine high-throughput scanning SAXS/WAXS experiments similar to existing laboratory instruments (Jakob *et al.*, 2003), but with a considerably smaller beam size and shorter data acquisition time.

Hard X-ray microbeams have already been produced at bending magnet or wiggler sources (Iida & Takashi, 1993; Mosbah *et al.*, 1999; Žižak *et al.*, 2000; Nozue *et al.*, 2003). A new microfocus beamline has recently been designed (Erko *et al.*, 2004) and commissioned at the 7 T wavelength-shifter source at BESSY II in Berlin (Germany). An experimental station has been developed and installed, with the goal of implementing a microbeam scanning instrument for the combination of simultaneous SAXS, WAXS and X-ray fluorescence (XRF) from thin sample sections. This unique combination of methods allows mapping of structural parameters from the atomic/molecular to the nanometre scale by combined SAXS and WAXS, simultaneously with chemical composition by XRF. The lateral resolution for SAXS/WAXS applications is given by the minimum beam size in the order of 5–10 μm. Here we present the 'μ-Spot' beamline and the experimental station layout for scanning SAXS/WAXS/XRF, together with first commissioning results in terms of beam size, flux, accessible range of scattering vectors and SAXS resolution.

2. Microfocus beamline

The beamline was constructed and installed by ACCEL instruments GmbH as a second branch (40 mrad off-centre) of the 7 T wavelength-shifter at the third-generation synchrotron radiation source BESSY II, utilizing the optical hutch of the BAM*line* (Gorner *et al.*, 2001). The accessible energy range is 1.9–30 keV, provided by a fixed exit double crystal monochromator with three sets of crystals (Si 111, Si 311 and Ge 111). The energy resolution can be varied between $\Delta E/E = 10^{-4}$ (Si 311) and $\Delta E/E = 10^{-2}$ (Si/W multilayer on Si 311). Several flexible optical schemes make it a multi-purpose beamline for applications in X-ray scattering and X-ray spectroscopy (Erko *et al.*, 2004). For scanning microbeam small-angle X-ray scattering (SAXS), both a small beam at the sample position and a low divergence are required at a reasonable flux. Mainly two options have been tested so far for scanning microbeam SAXS/WAXS at the microfocus beamline at BESSY II (Fig. 1).

Table 1
Comparison of the beamline performance for the two options for microbeam SAXS/WAXS. The beam size (FWHM) was measured at the sample position and, for the sake of comparison, the flux through a 10 μm pinhole was measured for both options with a calibrated photodiode. The divergence is determined by the acceptance of the BFL and the bimorph mirror M2 for option (*a*), and by the horizontal acceptance of the torroidal mirror M1 and the vertical acceptance of the multilayer monochromator for option (*b*).

	Energy (keV)	Size (μm) ($h \times v$)	Flux (photons s^{-1} 10 μm 100 mA^{-1})	Divergence (mrad) ($h \times v$)
Option (*a*)	9.0	18 × 16	1.7×10^8	0.6 × 1.0
Option (*b*)	15.0	15 × 11	2.0×10^9	1.0 × 0.1

Option (*a*). This option uses a bimorph mirror (Signorato, 2004) 30 m from the source for vertical focusing, and linear Bragg–Fresnel lenses (BFL) on the (Ge 111) second crystal of the monochromator for horizontal focusing (Fig. 1*a*). Five BFL, fabricated using a new metal coating technique (Firsov *et al.*, 2001), were installed for energies of 4, 7, 9, 16 and 24 keV. This focusing scheme was designed to provide a divergence < 1 mrad (both horizontally and vertically) and a beam size of roughly 10 μm at a flux of 10^9 photons s^{-1} 100 mA^{-1} (Erko *et al.*, 2004). The toroidal mirror M1 can not be used for pre-focusing in this option due to its large aberrations.

Option (*b*). In this option, the beam is focused by the toroidal mirror M1 located 13 m from the source with a 1:1.53 magnification. This provides a beam of about 300 μm size (determined by the surface quality of the mirror) at the focus position with a divergence of 1 mrad × 0.25 mrad ($h \times v$). The microbeam is then defined using M1 together with the double multilayer monochromator (DMM) and a beam-defining pinhole close to the sample (Fig. 1*b*). The broad energy band from the monochromator and the pre-focusing with M1 permit a higher flux compared with option (*a*). An advantage of this option is also the simple setup and the high position stability of the beam. A disadvantage is the rather broad bandwidth ($\Delta E/E \approx 10^{-2}$) which, by analogy with small-angle neutron scattering (SANS), leads to a *q*-dependent ($q = 4\pi \sin\theta/\lambda$, with the X-ray wavelength λ and the scattering angle 2θ) smearing of the intensity (Pedersen *et al.*, 1990).

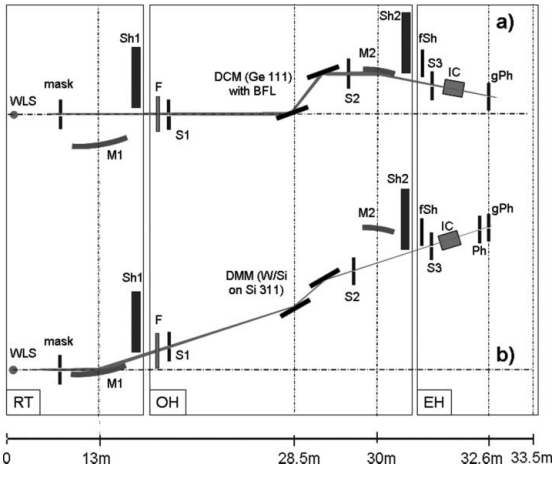

Figure 1
Optical layout of the μ-Spot beamline with the two options (*a*) and (*b*) used for scanning SAXS/WAXS. M1: toroidal mirror; M2: bimorph mirror, DCM: double crystal monochromator with linear Bragg–Fresnel lenses; DMM: double multilayer monochromator; Ph: beam-defining pinhole for option (*b*); gPh: guard pinhole close to the sample position; WLS: 7 T wavelength-shifter source; S1, S2 and S3: slit systems; F: Filter; Sh: beam shutters; fSh: fast shutter for triggering with the MarMosaic detector; IC: ionization chamber; RT: ring tunnel; OH: optics hutch; EH: experimental hutch. The distance between the sample and the SAXS/WAXS detector in the experimental hutch can be varied continuously between 0.1 m and 0.9 m.

The beamline performance for SAXS/WAXS was evaluated for the two options described above for selected energies. The BFL/bimorph mirror combination [option (*a*)] was tested at an energy of 9 keV. A minimum beam size of roughly 15 μm (full width at half maximum, FWHM) could be reached at the focal position (see Table 1), although with a lower flux, as expected from ray-tracing calculations. In particular, the vertical focusing by the bimorph mirrors may be significantly improved by an automated optimized mirror-bending routine. Moreover, a new BFL with smaller zone width will be installed, which should increase the flux by a factor of four. Fig. 2 shows the flux from the multilayer monochromator as a function of energy for the beam focused with the toroidal mirror [option (*b*)]. For the maximum ring current of 250 mA, it delivers an intensity of about 10^{13} photons s^{-1} focused to a beam size smaller than 0.5 mm at the sample position. Therefore, this option can be used for fast time-resolved SAXS/WAXS experiments as well as for diffuse scattering from weakly scattering samples without using the microfocus option. To obtain a microbeam, a beam-defining pinhole is inserted close to the sample position. A pinhole of 10 μm diameter, together with a guard pinhole (20 μm diameter) 5 mm apart, delivers a smaller beam at the sample position than option (*a*) with roughly an order of magnitude higher flux (Table 1). This enables at present option (*b*) for scanning SAXS/WAXS applications, also in view of the higher position stability of the beam, which in this case is solely defined by the stability of the pinhole support.

3. The SAXS/WAXS/XRF experimental station

3.1. Experimental setup

A sketch of the experimental station is shown in Fig. 3. The whole instrument is placed on a Newport table (2000 mm × 1500 mm) which can be vertically translated to fit the beam heights for the different optical schemes [see Fig. 1 and Erko *et al.* (2004)]. The sample stage consists of an *xyz* translation stage (right-handed system with *x* = beam direction) and a θ–2θ goniometer. Microbeam scanning is provided by an additional small *xyz* scanning stage with linear encoders (resolution 100 nm) on top of the goniometer. The whole goniometer, as well as the SAXS/WAXS detector, can be moved

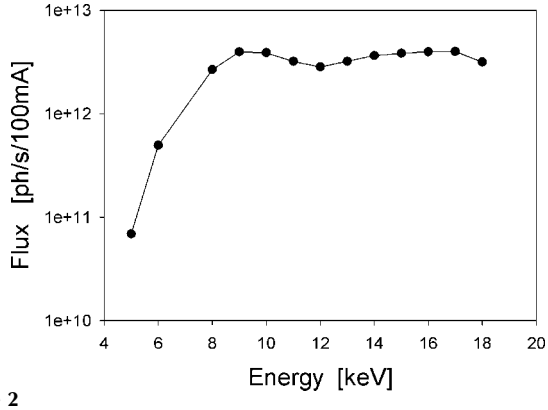

Figure 2
Flux at the sample position for the X-ray beam focused with the toroidal mirror M1 and monochromated by the W/Si multilayer. The beam size at the focal position is about 300 μm × 500 μm ($h \times v$). The decrease towards small energies is due to absorption in air (about 300 mm air path), and the dip at around 12 keV is due to the W *L* absorption edges of the multilayer.

independently along the x direction, and the SAXS/WAXS detector can additionally be moved vertically (z direction) to maximize the simultaneously accessible q range. Due to space restrictions in the experimental hutch, the maximum sample to detector distance is about 1 m. A beam-defining pinhole can be mounted on a motorized five-axis stage (three translations and two tilts), and a motorized two-axis stage with a guard pinhole can be placed close (< 1 mm distance) to the sample to minimize parasitic scattering from air and from the beam-defining pinhole. A long-distance optical microscope (Infinity Optical, Boulder, USA) with a resolution of 2.2 µm and a field of view of 1.6 mm is mounted on the 2θ goniometer arm and allows observation of the specimen on-axis (*i.e.* parallel to the X-ray beam) for the definition of scan positions and/or regions of interest on the specimen. In an off-axis position (*e.g.* at 45°), on-line observation of the specimen during X-ray data collection is also possible. The position calibration of the X-ray beam at the sample position is performed with a high-resolution $CdWO_4$ crystal on a 1 mm thick glass substrate, which can be directly viewed on-axis with the optical microscope. Since the crystal is mounted by default on the high-resolution scanning stage parallel to the specimen, the beam position can be checked and calibrated with respect to the absolute sample position very easily at any time with only a short interruption of the experiment. The reproducible accuracy of the absolute beam position is of the order of 2 µm, mostly given by the resolution of the $CdWO_4$ crystal and the optical microscope. The SAXS/WAXS detector is a MarMosaic 225 (Mar USA, Evanston, USA), consisting of nine independent 16-bit CCD chips connected to a phosphor screen of 225 mm edge length with fibre optic tapers. The width of the point spread function is $\approx$ 100 µm, the pixel size is 73.24 µm and the readout time at full resolution is < 5 s. In addition to the MarMosaic detector for SAXS/WAXS, an energy-sensitive detector (Röntec X-flash, Berlin, Germany) is placed in back-reflection geometry at about 135° (Fig. 3*b*) in order to collect simultaneously the X-ray fluorescence spectrum for each scanning point on the specimen. Alternatively, the X-flash detector can be used to measure the fluorescence signal from the beamstop (*e.g.* the Pb L lines). Together with an ionization chamber in front of the specimen, this allows the determination of the sample transmission for each point during a scanning SAXS/WAXS experiment. Alternatively, an absolutely calibrated photodiode can be inserted under remote control into the direct beam for transmission measurement and for primary flux determination.

For microbeam SAXS/WAXS applications, the normal beamline operation is in air, with a very small beamstop placed as close as possible to the sample position to avoid air scattering (Fig. 3*b*) (Riekel *et al.*, 2000). For high-flux SAXS applications with a larger beam size, insertion of a 500 mm long He-filled flight tube with the beamstop directly mounted on the Kapton outlet window has also been successfully tested. The specimen is usually mounted on a small goniometer head using a magnetic base system, but any other specimen holder can easily be adapted. For large custom made (*in-situ*) setups, the high-resolution scanning table has to be replaced by the respective setup. A cryo-jet system (KGW, Karlsruhe, Germany) with liquid N_2 is installed at the station and can be used by default for

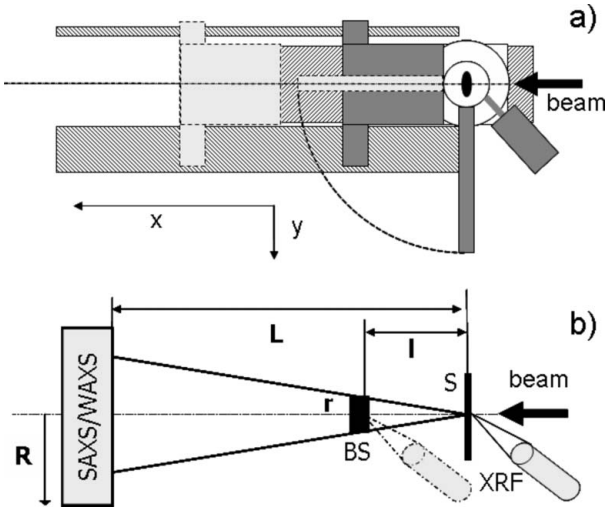

Figure 3
(*a*) Top-view sketch of the experimental station, with main components: sample goniometer (white) with scanning stage (black), detector and goniometer translation stages (hatched), and detectors (SAXS/WAXS detector, XRF detector and optical microscope, dark grey). The light grey shows the microscope rotated into the beam, with the SAXS/WAXS detector in its parking position. (*b*) Definition of the major geometric parameters for SAXS/WAXS: distance l between sample (S) and beamstop (BS); distance L between sample and SAXS/WAXS detector, SAXS/WAXS detector size $2R$ and beamstop size $2r$. The XRF detector is placed in back-reflection geometry and points either to the sample or to the beamstop (see text).

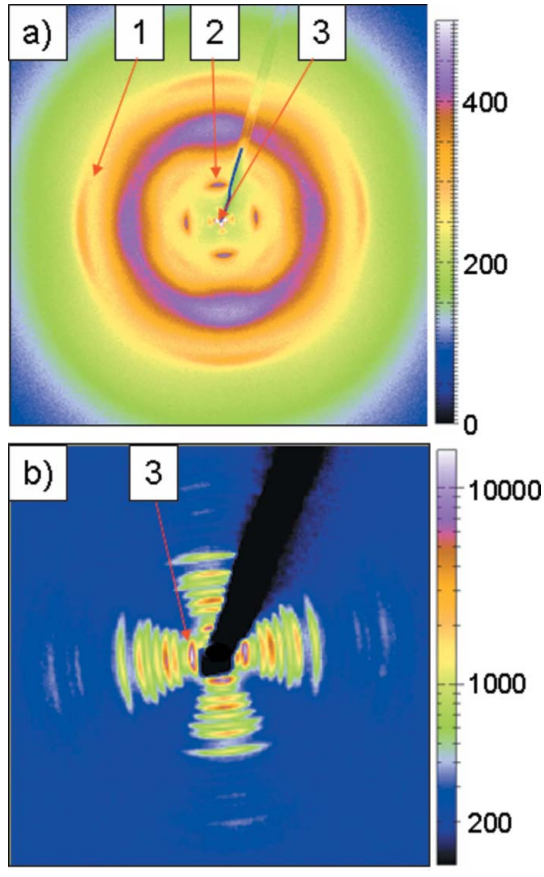

Figure 4
Two-dimensional SAXS/WAXS pattern from two crossed rat tail collagen fibres (raw data, no background subtracted). The numbers correspond to different reflections described in the text. The setup used for the measurement was option (*b*) with a 10 µm beam-defining pinhole, a wavelength of λ = 0.827 Å and a sample to detector distance of L = 253 mm. The beamstop consisted of a lead wire of 0.25 mm diameter at a distance of about 50 mm from the sample. (*a*) shows the whole pattern with the maximum scattering angle corresponding to $2\theta = 32°$, and (*b*) shows the enlarged central region of (*a*) with the meridional reflections from dry collagen type II (d = 650 Å) up to the 20th order. The total q range is 0.2 $nm^{-1} < q < 40$ nm^{-1}.

Table 2
SAXS resolution at $q \approx 0$ for different setups. The width of the resolution function W was approximated by a Gaussian fit of the second- or third-order collagen reflections (see Fig. 4*b*) (Fratzl *et al.*, 1993).

Option	E (keV)	L (mm)	W_H (nm^{-1})	W_V (nm^{-1})
(*a*)	9	161	–	0.061
(*b*)	15	253	0.063	0.061
(*b*)	15	817	0.065	0.022

radiation-sensitive specimens. Finally, biological specimens can be prepared on-site in a newly constructed preparation laboratory near to the beamline, allowing, for instance, the direct transfer of native cryo-sectioned tissues to the cryo-stream facility at the instrument. First tests have demonstrated the feasibility of cryo-stream cooling in combination with microbeam SAXS/WAXS scanning of samples of several mm in size.

The beamline and the experimental station are controlled by *SPEC* (Certified Scientific Software, USA), partly on top of an *EPICS* control system which operates all beamline motors and some of the motors in the experimental hutch. A Python-based graphical user interface (GUI), including tools for online data analysis and interactive instrument control, is currently under development.

3.2. Accessible q range and resolution for simultaneous SAXS/WAXS

Fig. 4 shows a two-dimensional SAXS/WAXS pattern from two crossed rat tail tendon collagen fibres. Features from three hierarchical levels are recognized simultaneously, *i.e.* the meridional helix diffraction peak at 2.9 Å from the triple helical molecules (1), the equatorial ordering peak from the lateral order of the collagen fibrils at 11.5 Å (2) and the third-order reflection from the lateral staggering of the collagen molecules at 217 Å (3) [see *e.g.* Wess (2005)].

Most SAXS instruments are designed for optimum resolution in reciprocal space and thus the beam is usually focused onto the detector. For microbeam applications, however, the focus lies preferentially at the sample position, and a compromise has to be found between a minimum beam size and an optimum SAXS resolution. The SAXS resolution can be estimated by assuming Gaussian functions for the beam profile as well as for the detector point spread function (Pedersen *et al.*, 1990). Taking into account that the beam size at the focal position (*i.e.* at the sample position, $B \approx 10$ µm) is much smaller than the detector point spread function ($P \approx 100$ µm for the MarMosaic 225), the width (full width at half maximum, FWHM) of the (Gaussian) resolution function can be approximated by

$$W_0 \simeq \frac{2\pi}{\lambda}\sqrt{\alpha^2 + \left(\frac{P}{L}\right)^2} \qquad (1)$$

with the beam divergence angle α and the sample–detector distance L. Taking a maximum divergence of $\alpha \approx 1$ mrad (Table 1), a value of $W_0 \simeq 0.08$ nm^{-1} is estimated for a wavelength of $\lambda = 0.827$ Å and $L = 253$ mm (Fig. 4). Experimentally determined values for W_0 derived from the width of the meridional collagen reflections are given in Table 2 for different setups.

An interesting aspect in Table 2 is that for the given values of divergence and detector point spread function, the horizontal resolution is practically independent of the sample–detector distance L for $L > 200$ mm. This is also clear from equation (1), which implies that for very small X-ray beams in the micron range and a detector with high spatial resolution, the reciprocal space resolution is, for practical sample–detector distances, determined by the beam divergence. This allows the construction of very compact SAXS instruments (Riekel *et al.*, 2000) and, moreover, it allows simultaneous SAXS/WAXS measurements over a wide q range. For the example shown in Fig. 4, a maximum value of $q_{max} = 40$ nm^{-1} can be reached at about 250 mm sample–detector distance. Together with a minimum value of $q_{min} \simeq 0.2$ nm^{-1}, this simultaneously yields a factor of 200 in q range. The practical value of q_{min} is determined by the size of the beamstop (Fig. 3*b*), which should be placed as close as possible to the sample in order to minimize air scattering from the direct beam. The value of q_{min} can be pushed further to about 0.1 nm^{-1} by increasing the sample–beamstop distance l (Fig. 3*b*), or preferably by using an even smaller beamstop, since the reduction of air scattering is a serious issue when investigating weakly scattering samples of a few microns thickness. A beamstop with a diameter of 125 µm is currently being tested. Together with a shorter sample–detector distance of $L \approx 100$ mm, a simultaneous q range of nearly a factor of 1000 is feasible in principle.

For a finite wavelength spread of the radiation, the SAXS/WAXS resolution contains an additional term which, in contrast with the angular contribution, is q-dependent. For Gaussian distributions, the total width is then (Pedersen *et al.*, 1990)

$$W_{Tot} \approx \sqrt{W_0^2 + \left(q\frac{\Delta\lambda}{\lambda}\right)^2}, \qquad (2)$$

with W_0 given by equation (1). Fig. 5 shows as an example the vertical width W_{Tot} as a function of q for option (*b*), obtained from Gaussian fits of the reflections from a silver behenate powder sample (Huang *et al.*, 1993) and from rat tail tendon collagen (Fig. 4). The one-dimensional SAXS profiles were obtained by azimuthal averaging of a narrow (±10°) vertical sector of the two-dimensional patterns. The fits to the experimentally determined peak widths with equation (2) (lines in Fig. 5) give $\Delta\lambda/\lambda = 0.012$, in good agreement with the nominal energy resolution of the multilayer of 1%, and $W_0 = 0.022$ nm^{-1} for the collagen sample. For collagen, the width of the reflections extrapolated to $q = 0$ can be taken as a good approximation for the angular resolution of the instrument (Fratzl *et al.*, 1993). In contrast, the reflections from silver behenate are strongly

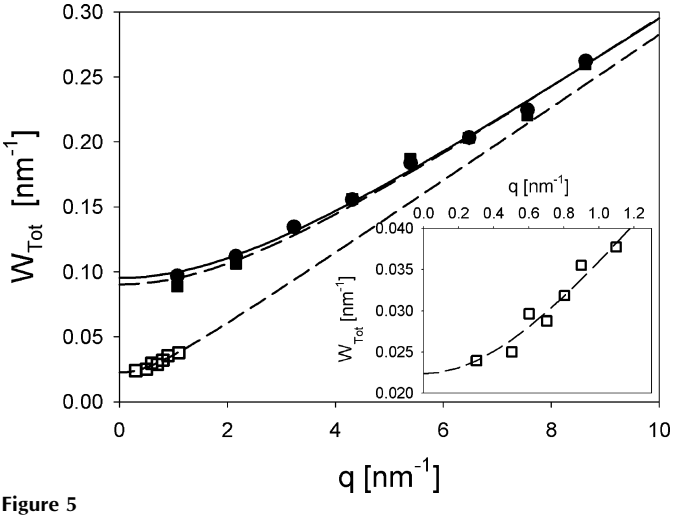

Figure 5
Vertical SAXS resolution for option (*b*) at $E = 15$ keV and $L = 817$ mm with a 100 µm beam-defining pinhole (squares) and a 10 µm beam-defining pinhole (circles) from silver behenate (black symbols) and rat tail tendon collagen (open symbols). The lines are fits to the data with equation (2) and give $\Delta\lambda/\lambda = 0.012$ (note that the fitted curves are all parallel for large q) and $W_0 = 0.022$ nm^{-1} for the collagen sample, and $W_0 \simeq 0.095$ nm^{-1} for the silver behenate sample. The inset shows an enlargement of the rat tail tendon data with the corresponding fit.

broadened due to the very small crystallite size (Huang *et al.*, 1993). Using the W_0 value from collagen as the width of the instrument resolution function, the size of the crystallites is estimated to be 700 Å by applying the Scherrer approximation.

4. Conclusion

A new instrument for simultaneous SAXS/WAXS/XRF is operational at the microfocus beamline at BESSY II. The beamline provides an energy range of 1.9–30 keV with a microbeam down to 10 µm at a flux of about 10^9 photons s^{-1} at intermediate energies. Two microbeam options are currently available. Option (*a*) uses linear Bragg–Fresnel lenses and a bimorph mirror combination, and option (*b*) uses a toroidal mirror in combination with a multilayer monochromator and a beam-defining pinhole. At present, option (*b*) exhibits better performance in terms of flux and stability, but leads to a *q*-dependent smearing due to the finite wavelength spread of the multilayer monochromator. A SAXS resolution of up to 500 Å *d*-spacing and a range of scattering vectors of almost three orders of magnitude can be reached using a high-resolution CCD-based detector for simultaneous SAXS/WAXS. The long-term goal is to proceed from microbeam scanning experiments to a real imaging technique. For a user-friendly 'scanning SAXS/WAXS/XRF microscope' in routine operation, one of the major future tasks in this respect is the development of sophisticated software for interactive instrument control combined with online data analysis and online parameter mapping.

We are grateful to A. Gourrier and H. Gupta (MPI, Potsdam) and to C. Riekel and M. Burghammer (ESRF, Grenoble) for many helpful discussions and for their contributions on software developments. We thank B. Kanngießer and W. Malzer (TU Berlin), I. Packe (BESSY), and M. Radtke and K. Wenzel (BAM) for many discussions on the design and construction of the experimental station. The mechanical and electrical workshops at BESSY, BAM and MPI are acknowledged for technical support and the BESSY-IT team are thanked for their help with the implementation of devices into *EPICS*. We acknowledge financial support from the Max Planck Society, the Federal Institute for Materials Research and Testing (BAM), BESSY GmbH and the BMBF (Project No. 05KS4KT1/6).

References

Aizenberg, J., Weaver, J. C., Thanawala, M. S., Sundar, V. C., Morse, D. E. & Fratzl, P. (2005). *Science*, **309**, 275–278.
Currey, J. D. (1999). *J. Exp. Biol.* **202**, 3285–3294.
Erko, A., Schaefers, F., Firsov, A., Peatmann, W. B., Eberhardt, W. & Signorato, R. (2004). *Spectrochimica Acta B*, **59**, 1543–1548.
Firsov, A., Svintsov, A., Erko, A., Gudat, W., Asryan, A., Ferstl, M., Shapoval, S. & Aristov, V. (2001). *Nucl. Instrum. Methods A*, **467**, 366–369.
Fratzl, P. (2003). *J. Appl. Cryst.* **36**, 397–404.
Fratzl, P., Gupta, H. S., Paschalis, E. P. & Roschger, P. (2004). *J. Mater. Chem.* **14**, 2115–2123.
Fratzl, P., Jakob, H. F., Rinnerthaler, S., Roschger, P. & Klaushofer, K. (1997). *J. Appl. Cryst.* **30**, 765–769.
Fratzl, P., Langmayr, F. & Paris, O. (1993). *J. Appl. Cryst.* **26**, 820–826.
Gorner, W., Hentschel, M. P., Muller, B. R., Riesemeier, H., Krumrey, M., Ulm, G., Diete, W., Klein, U. & Frahm, R. (2001). *Nucl. Instrum. Methods A*, **467**, 703–706.
Huang, T. C., Toraya, H., Blanton, T. N. & Wu, Y. (1993). *J. Appl. Cryst.* **26**, 180–184.
Iida, A. & Takashi, N. (1993). *Nucl. Instrum. Methods B*, **82**, 129–138.
Jakob, H. F., Erlacher, K. & Fratzl, P. (2003). *Mater. Sci. Forum*, **41**, 411–418.
Jaschouz, D., Paris, O., Roschger, P., Hwang, H. S. & Fratzl, P. (2003). *J. Appl. Cryst.* **36**, 494–498.
Kamat, S., Su, X., Ballarini, R. & Heuer, A. H. (2000). *Nature*, **405**, 1036–1040.
Lichtenegger, H., Muller, M., Paris, O., Riekel, C. & Fratzl, P. (1999). *J. Appl. Cryst.* **32**, 1127–1133.
Loidl, D., Peterlik, H., Paris, O., Müller, M., Burghammer, M. & Riekel, C. (2005). *J. Synchrotron Rad.* **12**, 758–764.
Mosbah, M., Duraud, J. P., Metrich, N., Wu, Z., Delaney, J. S. & San Miguel, A. (1999). *Nucl. Instrum. Methods B*, **158**, 214–220.
Nozue, Y., Kurita, R., Hirano, S., Kawasaki, N., Ueno, S., Iida, A., Nishi, T. & Amemiya, Y. (2003). *Polymer*, **44**, 6397–6405.
Paris, O., Žižak, I., Lichtenegger, H., Roschger, P., Klaushofer, K. & Fratzl, P. (2000). *Cell. Mol. Biol.* **46**, 993–1004.
Pedersen, J. S., Posselt, D. & Mortensen, K. (1990). *J. Appl. Cryst.* **23**, 321–333.
Riekel, C. (2000). *Rep. Prog. Phys.* **63**, 233–262.
Riekel, C., Burghammer, M. & Müller, M. (2000). *J. Appl. Cryst.* **33**, 421–423.
Riekel, C. & Davies, R. J. (2005). *Curr. Opin. Collect. Interf. Sci.* **9**, 396–403.
Signorato, R. (2004). *Am. Inst. Phys. Conf. Proc.*, **705**, 812–818.
Wagermaier, W., Gupta, H. S., Gourrier, A., Paris, O., Roschger, P., Burghammer, M., Riekel, C. & Fratzl, P. (2007). *J. Appl. Cryst.* **40**. In the press.
Weiner, S. & Wagner, H. D. (1998). *Annu. Rev. Mater. Sci.* **28**, 271–298.
Wess, T. J. (2005). *Adv. Protein Chem.* **70**, 341–374.
Žižak, I., Paris, O., Roschger, P., Bernstorff, S., Amenitsch, H., Klaushofer, K. & Fratzl, P. (2000). *J. Appl. Cryst.* **33**, 820–823.
Žižak, I., Roschger, P., Paris, O., Misof, B. M., Berzlanovich, A., Bernstorff, S., Amenitsch, H., Klaushofer, K. & Fratzl, P. (2003). *J. Struct. Biol.* **141**, 208–217.